Frequency-Differencing Method to Kickstart Waveform Inversion Without Cycle Skipping

Rehman Ali, Trevor Mitcham, Nebojsa Duric
Department of Imaging Sciences, University of Rochester Medical Center, Rochester, NY, USA
Email: Rehman_Ali@URMC.Rochester.edu, Trevor_Mitcham@URMC.Rochester.edu, Nebojsa_Duric@URMC.Rochester.edu

2024 IEEE Ultrasonics, Ferroelectrics, and Frequency Control Joint Symposium (UFFC-JS) | 979-8-3503-7190-1/24/$31.00 ©2024 IEEE | DOI: 10.1109/UFFC-JS60046.2024.10794178

***Abstract*—Because of its fast reconstruction times, frequency-domain full waveform inversion is the clinical gold standard for high-resolution sound speed imaging in medical ultrasound tomography; however, it fundamentally relies on having sufficiently low-frequency data to avoiding cycle skipping. This motivates the development of new strategies that can overcome cycle skipping in the absence of low-frequency data. In this work, we synthesize approximate low-frequency content from existing high-frequency signals using the same frequency differencing method used in frequency-difference beamforming for underwater sonar. The approximate low-frequency content is then used to kickstart full-waveform inversion so that cycle skipping can be better avoided at higher frequencies. We demonstrate the efficacy of this new approach using in-vivo breast imaging cases. In each case, internal tissue structures are seen with much greater clarity without cycle skipping artifacts when frequency differencing is used to provide a starting model for conventional full-waveform inversion.**

***Index Terms*—Ultrasound Tomography, Full Waveform Inversion, Frequency Difference Beamforming**

I. INTRODUCTION

Ultrasound tomography (UST) uses the transmission of ultrasound through tissue to reconstruct high-resolution images of tissue properties such as sound speed and attenuation. The most common clinical use of UST is breast imaging [1]–[4] where sound speed and attenuation serve as biomarkers for cancer detection. The full waveform inversion (FWI) algorithm responsible for high-resolution UST imaging relies on the accurate simulation of pressure fields in a heterogeneous medium. For the application to breast imaging, FWI often requires low-frequency signals (less than 1 MHz) to overcome cycle skipping caused by errors in a starting model. This is because FWI directly minimizes the error between simulated and measured signals. If the simulated signal is delayed or time-advanced by more than a half cycle relative to the measured signal, the underlying model used in the simulation will update in the wrong direction due to cycle skipping. Low frequencies lengthen this half-cycle window, allowing FWI to overcome errors in a starting model [5].

By contrast, most ultrasound transducer designs are driven towards high frequencies by the need to maximize the resolution achievable by B-mode reflectivity imaging. Because full-waveform inversion (FWI) requires low frequencies to overcome cycle skipping, it is often difficult to apply FWI to the same high-frequency transducer hardware. Therefore, the lack of low-frequency signal content on most ultrasound transducers currently designed for B-mode imaging prevents FWI from becoming more broadly applicable.

Recent work on time-domain adaptive waveform inversion (AWI) addresses this based on a deconvolution approach to overcome cycle skipping [6]–[8]. Adaptive waveform inversion (AWI) overcomes the dependence on low frequencies by modeling the mismatch between simulated and measured signals as a bank of impulse responses [6]. Rather than directly minimizing the error between simulated and measured signals, AWI drives these impulse responses toward zero-time lag, circumventing the cycle skipping problem. However, the main difficulty limiting AWI is its time-domain methodology as most clinical UST scanners rely on frequency-domain FWI for fast image reconstruction [4], [9].

Fortunately, time lag is equivalent to a linear phase response in the frequency domain, so a frequency-domain implementation of AWI can be achieved by flattening this linear phase response. One way this can be achieved is by using a mathematical trick from sonar known as frequency-differencing [10]. By taking the ratio of signals at two different frequencies f_1 and f_2, we can produce a new signal at frequency difference $\Delta f = |f_1 - f_2|$. By minimizing the error between simulated and measured signals after frequency differencing, cycle skipping can be overcome by using a sufficiently small frequency difference Δf.

Therefore, although the broadband nature of AWI makes it difficult to translate to the frequency domain, we can approximate the properties of AWI by using a frequency-differencing approach, which we previously investigated [11]. This previous work describes both a model-domain and a data-domain method for frequency-differencing. The model-domain approach reconstructs sound speed by modeling the ratio of signals at two different frequencies and performing the model inversion in terms of this ratio. In the data-domain approach, conventional FWI is applied to low-frequency content at frequency Δf generated by taking a ratio of integrals over multiple frequency pairs. While the model-domain approach changes the underlying model used during the inversion process, the data-domain approach assumes that conventional FWI is sufficient to model the signal synthesized at Δf. Although the dual-frequency model-domain approach was more accurate, the model was often ill-conditioned for inversion, especially in low signal-to-noise ratio settings. On the hand, the data-domain approach often yielded low-resolution images but was far more robust to the presence of noise. In this work, we focus on the data-domain method of frequency differencing and apply it to in-vivo breast UST data, where noise and tissue heterogeneities are significant challenging factors. Each breast imaging case show that the frequency-differencing approach helps overcome cycle skipping by providing a sufficiently accurate starting model for FWI.

II. Theory and Methods

A. Frequency-Domain FWI Using the Helmholtz Equation

Using finite difference methods [12], we solve the 2D Helmholtz equation to obtain a pressure field $\mathbf{u}$ for a given source δ, frequency $\omega = 2\pi f$, and slowness $\mathbf{s}$ (i.e., the reciprocal of sound speed):

$$(\nabla^2 + \omega^2 \mathbf{s}^2)\mathbf{u}(\omega, \mathbf{s}) = \delta(\omega), \tag{1}$$

After discretization, the $(\nabla^2 + \omega^2 \mathbf{s}^2)$ operator becomes a sparse matrix A that encodes the finite difference scheme so that equation (1) can be described using the following matrix-vector formulation (where $\mathbf{u}$ and δ are now vectors over spatial locations on the discretized grid):

$$A(\omega, \mathbf{s})\mathbf{u}(\omega, \mathbf{s}) = \delta(\omega), \tag{2}$$

Differentiating both sides of this equation with respect to s gives us:

$$\frac{\partial \mathbf{u}}{\partial \mathbf{s}} = -A^{-1}\frac{\partial A}{\partial \mathbf{s}}\mathbf{u} = -A^{-1}\frac{\partial A}{\partial \mathbf{s}}A^{-1}\delta, \tag{3}$$

Rather than observing the full pressure field $\mathbf{u}$ at all locations in space, we only observe the pressure field $\mathbf{p}$ at the ring array. The relationship between $\mathbf{p}$ and $\mathbf{u}$ is: $\mathbf{p} = K\mathbf{u}$, where K is a sampling operator that extracts the pressure field at each element of the ring array. The relationship between changes in slowness and changes in the simulated pressure field at the ring array is

$$\frac{\partial \mathbf{p}}{\partial \mathbf{s}} = -KA^{-1}\frac{\partial A}{\partial \mathbf{s}}\mathbf{u} = -KA^{-1}\frac{\partial A}{\partial \mathbf{s}}A^{-1}\delta, \tag{4}$$

The cost function for waveform inversion is:

$$\begin{aligned} E(\omega, \mathbf{s}) &= \frac{1}{2}\sum_{i=1}^{N}\left\|\mathbf{p_i}(\omega, \mathbf{s}) - \mathbf{p_{obs,i}}(\omega)\right\|_2^2 \\ &= \frac{1}{2}\sum_{i=1}^{N}\left(\mathbf{p_i}(\omega, \mathbf{s}) - \mathbf{p_{obs,i}}(\omega)\right)^H\left(\mathbf{p_i}(\omega, \mathbf{s}) - \mathbf{p_{obs,i}}(\omega)\right), \end{aligned} \tag{5}$$

where $\mathbf{p_i}$ and $\mathbf{p_{obs,i}}$ are the simulated and observed pressure measurements on the ring array for the i^{th} single-element transmission $\delta_\mathbf{i}$ (i ranges from 1 to N, the number of elements on the ring array). The gradient of $E(\omega, \mathbf{s})$ with respect to slowness $\mathbf{s}$ is given by:

$$\begin{aligned} \nabla_\mathbf{s} E &= \sum_{i=1}^{N} Re\left\{\left(\frac{\partial \mathbf{p_i}}{\partial \mathbf{s}}\right)^H(\mathbf{p_i} - \mathbf{p_{obs,i}})\right\} \\ &= -\sum_{i=1}^{N} Re\left\{\left(\frac{\partial A}{\partial \mathbf{s}}\mathbf{u_i}\right)^H (A^H)^{-1}K^T(\mathbf{p_i} - \mathbf{p_{obs,i}})\right\}, \end{aligned} \tag{6}$$

This definition of the gradient is used to implement the conjugate gradient method as done in prior work [13], [14].

B. Complex Source Estimation for Frequency-Domain FWI

The waveform inversion described in the previous section assumes that the correct phase and amplitude is used for each single-element source $\delta_\mathbf{i}$; however, in practice, the phase and amplitude of each source must be estimated from measured waveform. The following projection formula provides a complex scaling γ_i that accounts for both the amplitude and phase from each source i:

$$\gamma_i = \frac{\mathbf{p_i}^H \mathbf{p_{obs,i}}}{\mathbf{p_i}^H \mathbf{p_i}} \tag{7}$$

The source vector and pressure fields are scaled to $\{\delta_\mathbf{i} \rightarrow \gamma_i \delta_\mathbf{i}\}$, $\{\mathbf{u_i} \rightarrow \gamma_i \mathbf{u_i}\}$, and $\{\mathbf{p_i} \rightarrow \gamma_i \mathbf{p_i}\}$, respectively.

C. Data-Domain Frequency Differencing

Data-domain frequency-differencing over the frequency band $\omega \in [\omega_{low}, \omega_{high}]$ yields the signal $\bar{\mathbf{p}}_\mathbf{obs,i}(\Delta\omega)$ at frequency difference $\Delta\omega$:

$$\bar{\mathbf{p}}_\mathbf{obs,i}(\Delta\omega) = \frac{\int_{\omega_{low}}^{\omega_{high}} \mathbf{p_{obs,i}}(\omega + \Delta\omega) \odot \mathbf{p}^*_\mathbf{obs,i}(\omega) d\omega}{\int_{\omega_{low}}^{\omega_{high}} \mathbf{p_{obs,i}}(\omega) \odot \mathbf{p}^*_\mathbf{obs,i}(\omega) d\omega}. \tag{8}$$

At this point, we can use the standard frequency-domain FWI algorithm with the following objective function:

$$E(\Delta\omega, \mathbf{s}) = \frac{1}{2}\sum_{i=1}^{N}\left\|\mathbf{p_i}(\Delta\omega, \mathbf{s}) - \bar{\mathbf{p}}_\mathbf{obs,i}(\Delta\omega)\right\|_2^2. \tag{9}$$

This objective function (9) is identical to the original FWI objective function (5), except that $\Delta\omega$ replaces ω and $\bar{\mathbf{p}}_\mathbf{obs,i}(\Delta\omega)$ replaces $\mathbf{p_{obs,i}}(\omega)$. In other words, a single Helmholtz equation at frequency $\Delta\omega$ is used to simulate $\mathbf{p_i}(\Delta\omega, \mathbf{s})$; however, rather than compare $\mathbf{p_i}(\Delta\omega, \mathbf{s})$ to actual content $\mathbf{p_{obs,i}}(\Delta\omega, \mathbf{s})$ at frequency $\Delta\omega$ (which may not be present with sufficient SNR in the recorded signal), we instead compare $\mathbf{p_i}(\Delta\omega, \mathbf{s})$ to $\bar{\mathbf{p}}_\mathbf{obs,i}(\Delta\omega)$ resulting from equation (8). The process used to generate $\bar{\mathbf{p}}_\mathbf{obs,i}(\Delta\omega)$ from existing data is very similar to what is used in frequency-difference beamforming [10] to overcome the same lack of low frequency content in existing signals.

D. Experimental Methods

Raw ultrasound channel data from an early whole-breast UST prototype [15] was used to reconstruct the speed of sound in the breast (data collected under IRB No. 040912M1F). The UST prototype system consists of a 22 cm diameter ring transducer with 1024 elements and a pulse center frequency of 2.5 MHz. The raw channel data (restricted to 512 elements, i.e., every other element) have been made publicly available for two different breast imaging cases [14]: https://github.com/rehmanali1994/WaveformInversionUST.

In each experiment, an ideal FWI, using frequencies ranging from 0.3 to 1.25 MHz, is used to reconstruct the sound speed starting from a homogeneous model of 1500 m/s. Then, the frequency used to start FWI is increased from 0.3 to 0.45 MHz to demonstrate cycle skipping. Next, FWI is applied to data

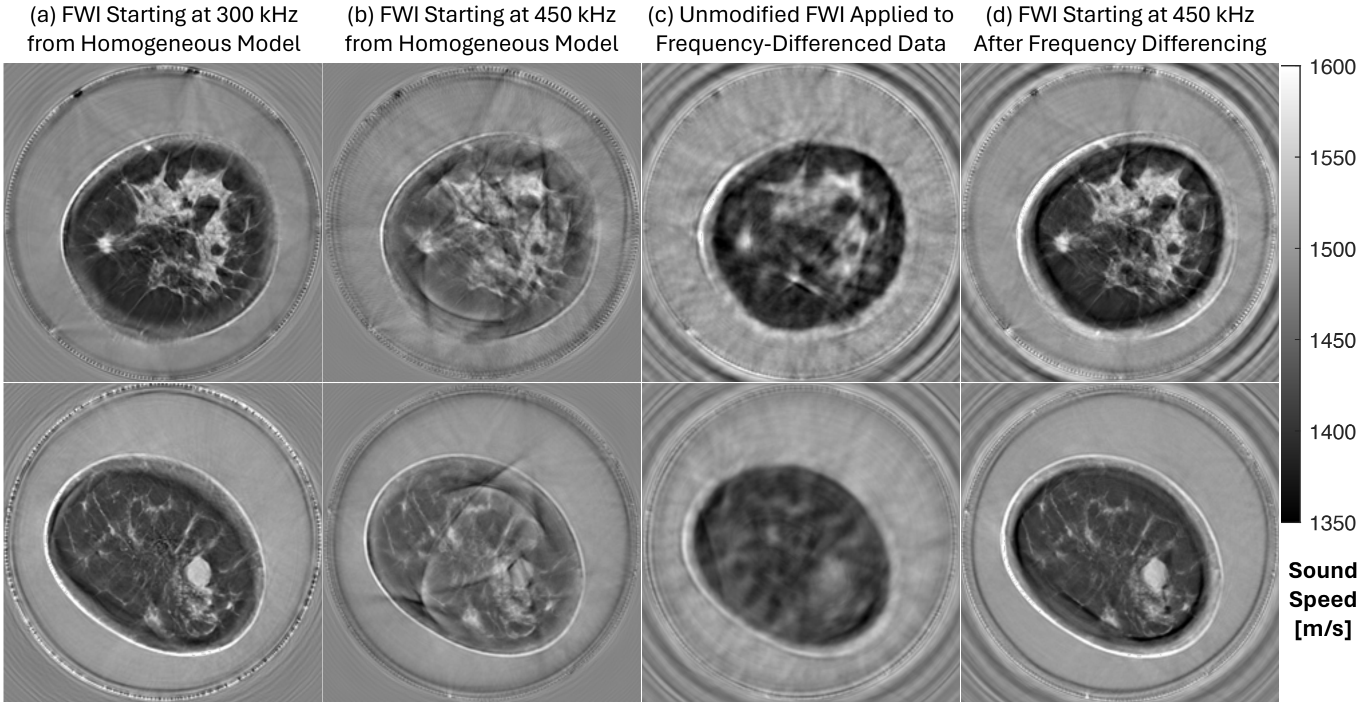

Fig. 1. Impact of data-domain frequency differencing on FWI in two different breast imaging cases. (a) Ideal FWI of the breast starting at 300 kHz from a homogeneous (1500 m/s) starting model. (b) Cycle-skipped FWI starting at 450 kHz from homogeneous model. (c) FWI applied to data generated from 100 to 450 kHz via frequency differencing. (d) FWI starting at 450 kHz after applying frequency-differencing to generate the initial sound speed estimate.

generated from 100 to 450 kHz via frequency differencing. Finally, the result of FWI applied to the frequency-differenced data is then used to replace the homogeneous starting model when FWI is applied starting at 450 kHz. The purpose of this final reconstruction is to show that frequency differencing can provide a sufficiently accurate starting model for overcoming cycle skipping in FWI.

III. Results and Discussion

Figure 1 demonstrates the frequency-differencing method in two different breast imaging cases. Figure 1(a) shows the ideal FWI when adequate low-frequency data (down to 300 kHz) is available. When FWI is started at 450 kHz (Figure 1(b)), structures inside the breast become obscured by cycle skipping artifacts. To overcome cycle skipping, FWI is applied to frequency-differenced data generated from 100 to 450 kHz (Figure 1(c)); although these images have low spatial resolution, they reveal the same internal tissue structure as seen with the ideal FWI. The main reason FWI reconstructs low-resolution images when applied to frequency-differenced data is that the simulation $\mathbf{p_i}(\Delta\omega, \mathbf{s})$ at frequency $\Delta\omega$ cannot fully replicate the frequency-differencing method or capture the physics at the multiple higher frequencies used in the frequency-differencing method. Despite this fundamental model mismatch, the result of applying FWI to frequency-differenced data can be used as the initial sound speed estimate for standard FWI starting at 450 kHz (i.e., using the raw data rather than the data generated by frequency differencing). In Figure 1(d), structures inside the breast can now be seen without cycle skipping.

IV. Conclusions and Future Work

Although the preliminary results show that the application of FWI to frequency-differenced data can overcome cycle skipping, the spatial resolution and accuracy of this approach is limited by the fundamental mismatch between the simulation model $\mathbf{p_i}(\Delta\omega, \mathbf{s})$ and the frequency-differenced data $\bar{\mathbf{p}}_{\mathbf{obs},\mathbf{i}}(\Delta\omega)$. There are two possible routes to overcoming this mismatch. The first option would be to incorporate model-domain frequency differencing into the simulation $\mathbf{p_i}(\Delta\omega, \mathbf{s})$ so that it accurately models the frequency difference calculation and all the frequencies used in the calculation. The second option would be retain the same model used in the standard frequency-domain FWI but to modify the frequency difference calculation (potentially via a deep learning approach [16]) so that it better capture the physics at a single low-frequency. Reducing the mismatch between the model and the data would further improve the efficacy of frequency differencing.

Acknowledgment

This work was funded by University of Rochester Medical Center and the National Institute of Biomedical Imaging and Bioengineering (NIBIB) under grants F32-EB034589 and R01-EB028652.

References

[1] C. Li, N. Duric, P. Littrup, and L. Huang, "In-vivo breast sound-speed imaging with ultrasound tomography," *Ultrasound in Medicine and Biology*, vol. 35, no. 10, pp. 1615–1628, 2009.

[2] N. Duric, P. Littrup, L. Poulo, A. Babkin, R. Pevzner, E. Holsapple, O. Rama, and C. Glide, "Detection of breast cancer with ultrasound tomography: First results with the computed ultrasound risk evaluation (CURE) prototype," *Medical physics*, vol. 34, no. 2, pp. 773–785, 2007.

[3] J. Schreiman, J. Gisvold, J. F. Greenleaf, and R. Bahn, "Ultrasound transmission computed tomography of the breast." *Radiology*, vol. 150, no. 2, pp. 523–530, 1984.

[4] J. Wiskin, D. Borup, S. Johnson, and M. Berggren, "Non-linear inverse scattering: high resolution quantitative breast tissue tomography," *The Journal of the Acoustical Society of America*, vol. 131, no. 5, pp. 3802–3813, 2012.

[5] R. Ali, T. Mitcham, and N. Duric, "Impact of starting model on waveform inversion in ultrasound tomography," in *Medical Imaging 2023: Ultrasonic Imaging and Tomography*, vol. 12470. SPIE, 2023, pp. 89–98.

[6] M. Warner and L. Guasch, "Adaptive waveform inversion: Theory," *Geophysics*, vol. 81, no. 6, pp. R429–R445, 2016.

[7] L. Guasch, M. Warner, and C. Ravaut, "Adaptive waveform inversion: Practice," *Geophysics*, vol. 84, no. 3, pp. R447–R461, 2019.

[8] L. Guasch, O. Calderón Agudo, M.-X. Tang, P. Nachev, and M. Warner, "Full-waveform inversion imaging of the human brain," *NPJ digital medicine*, vol. 3, no. 1, pp. 1–12, 2020.

[9] G. Sandhu, C. Li, O. Roy, S. Schmidt, and N. Duric, "Frequency domain ultrasound waveform tomography: breast imaging using a ring transducer," *Physics in Medicine & Biology*, vol. 60, no. 14, p. 5381, 2015.

[10] S. H. Abadi, H. Song, and D. R. Dowling, "Frequency-difference beamforming with sparse arrays," *The Journal of the Acoustical Society of America*, vol. 132, no. 3_Supplement, pp. 2082–2082, 2012.

[11] R. Ali, T. Mitcham, and N. Duric, "A new strategy to overcome cycle skipping: frequency-difference waveform inversion," in *Medical Imaging 2024: Ultrasonic Imaging and Tomography*, vol. 12932. SPIE, 2024, pp. 85–92.

[12] Z. Chen, D. Cheng, W. Feng, and T. Wu, "An optimal 9-point finite difference scheme for the helmholtz equation with pml." *International Journal of Numerical Analysis & Modeling*, vol. 10, no. 2, 2013.

[13] R. Ali, "Open-source full-waveform ultrasound computed tomography based on the angular spectrum method using linear arrays," in *Medical Imaging 2022: Ultrasonic Imaging and Tomography*, vol. 12038. SPIE, 2022, pp. 187–205.

[14] R. Ali, T. M. Mitcham, T. Brevett, Ò. C. Agudo, C. D. Martinez, C. Li, M. M. Doyley, and N. Duric, "2-d slicewise waveform inversion of sound speed and acoustic attenuation for ring array ultrasound tomography based on a block lu solver," *IEEE Transactions on Medical Imaging*, 2024.

[15] N. Duric, C. Li, O. Roy, and S. Schmidt, "Acoustic tomography: promise versus reality," in *2011 IEEE International Ultrasonics Symposium*. IEEE, 2011, pp. 2033–2041.

[16] O. Ovcharenko, V. Kazei, M. Kalita, D. Peter, and T. Alkhalifah, "Deep learning for low-frequency extrapolation from multioffset seismic data," *Geophysics*, vol. 84, no. 6, pp. R989–R1001, 2019.